Chin. Phys. Lett. **39**, 045201 (2022)

Atomically Dispersed Ni Single-Atoms Anchored on N-Doped Graphene Aerogels for Highly Efficient Electromagnetic Wave Absorption

Bing Suo(索冰), Xiao Zhang(张潇)*, Xinyu Jiang(姜心雨), Feng Yan(闫峰)*, Zhengzhi Luo(罗正智), and Yujin Chen(陈玉金)*

Key Laboratory of In-Fiber Integrated Optics (Ministry of Education), and College of Physics and Optoelectronic Engineering, Harbin Engineering University, Harbin 150001, China

(Received 15 December 2021; accepted 9 March 2022; published online 28 March 2022)

Uniformly dispersed nickel single atoms (SAs) are experimentally prepared on ultralight N-doped graphene aerogels (Ni-SA@NRGA). The experimental results show that Ni-SAs in graphene aerogels can improve the conduction, polarization losses, and impedance matching properties of the Ni-SA@NRGA. As a result, the minimum reflection loss ($R_{\mathrm{L,min}}$) of Ni-SA@NRGA is -49.46 dB with a matching thickness of 2.0 mm and the broadest efficient absorption bandwidth is 3.12 GHz at a low thickness of 1.5 mm. Meanwhile, even with a matching thickness of 1.2–2.0 mm, the $R_{\mathrm{L,min}}$ value of Ni-SA@NRGA can reach -20 dB. The current study demonstrates the significance of incorporating metal single atoms into graphene aerogel for electromagnetic wave absorption.

DOI: 10.1088/0256-307X/39/4/045201

The rapid development of high-frequency electronic devices causes electromagnetic pollution and interference, endangering human health and the living environment. Meanwhile, electromagnetic waves (EMWs) interfere with the normal operation of sensitive electrical devices.[1,2] To eliminate electromagnetic pollution and interference, researchers have developed various EMW absorbing materials such as ferrite, ceramics, carbon-based materials, conductive polymers, and magnetic metal particles over the last several decades. These traditional absorbing materials have some drawbacks such as narrow effective absorption bandwidth (EAB) and thick matching thickness.[3] As a result, it is important to develop EMW absorbing materials with low density, thin matching thickness, intense absorption ability, and wide absorption bandwidth.[4–7]

Graphene has become a research hotspot in EMW absorption (EWA) in recent years due to its superior specific surface area, low density, and high electrical conductivity.[8,9] However, if graphene is only used as an absorption material, it is difficult to tune its absorption bandwidth, impedance matching property, and absorption capacity.[9] Recently, it was found that fabrication of graphene aerogels (GAs) could significantly improve the EWA property of graphene-based absorbers. There were numerous hierarchical pores and three-dimensional (3D) networks in GAs, which not only gave a GA a high specific surface area and ultralow density but also effectively prevented the agglomeration of thin graphene sheets.[10] Furthermore, the multiple scattering of the EM wave in a GA makes it easier to improve the absorption property of the GA. Nevertheless, the absorption of pure GAs was not satisfactory due to lack of other loss factors. To increase dielectric loss factors, foreign magnetic nanomaterials such as Fe, Co, and Ni nanoparticles were introduced into GAs to increase the dielectric loss factors. For instance, Hu *et al.* synthesized 3D GA containing Fe_3O_4 nanocrystals, in which the synergistic effect between polarization and magnetic losses improved EWA performance.[11] Noticeably, the introduction of foreign materials increases the mass density and decreases the specific surface area of the GAs, affecting the lightweight property of the GA composites.

Metal single atoms (M-SAs) have recently received a great deal of attention in electrocatalysis because of their ultra-high surface free energy, high atomic dispersion, and high atomic utilization efficiency.[12] M-SAs coordinated with nitrogen species (M-N_x) anchored on the carbon matrix, in particular, have good stability and have been widely investigated for catalyzing various chemical reactions.[13] Because of the different electronegativities of the metal, nitrogen, and carbon atoms, electrons around M-N_x moieties would redistribute.[14] Electronic interactions between atoms and charge redistribution can change the electrical conductivity and create a local polarization system, which could promote the EWA property of the carbonaceous materials containing M-N_x moieties. More importantly, unlike nanoparticles, the introduction of M-SAs into nanocarbons has no significant effect on

*Corresponding authors: Email: chenyujin@hrbeu.edu.cn; yanfeng@hrbeu.edu.cn; zhangxiaochn@hrbeu.edu.cn
© 2022 Chinese Physical Society and IOP Publishing Ltd

mass density. As a result, M-SAs anchored nanocarbons have potential applications in lightweight EM absorbers. However, to the best of our knowledge, no high-performance GA containing uniform M-SAs has been reported so far.

In this study, we propose a simple method for anchoring Ni-SAs on the N-doped GAs (Ni-SA@NRGA) for EWA. The as-prepared Ni-SA@NRGA exhibits good absorption performance with thickness in the range of 1.5–5.0 mm, an EAB of 3.12 GHz, and an $R_{\mathrm{L,min}}$ of −49.46 dB at 10.64 GHz. The increased dielectric loss as well as the unique 3D porous structure of Ni-SA@NRGA contributes to its high absorption performance.

The NRGA, Ni-NP@NRGA, and Ni-SA@NRGA synthesis processes were thoroughly described in the Supplementary Material. The synthesis of Ni-SA@NRGA is depicted in Fig. 1. The graphene oxide was dispersed in distilled water using ultrasound, then hydrothermally treated at 180 ℃ for 10 h before being freeze-dried to form GAs. The mixture was then hydrothermally treated at 180 ℃ for 2 h with a piece of GAs, nickel chloride hexahydrate ($NiCl_2{\cdot}6H_2O$), and dicyandiamide (DCD) dispersed in 50 mL ethanol/water (volume : volume = 1 : 1). The sample obtained in this stage was annealed at 900 ℃ for 2 h to produce GAs containing Ni nanoparticles (Ni-NPs), denoted as Ni-NP@NRGA. Finally, the Ni-NP@NRGA was immersed in a 2 M H_2SO_4 solution to remove the Ni nanoparticles, and Ni-SA@NRGA was obtained. The digital photographs of the as-fabricated NRGA, Ni-NP@NRGA, and Ni-SA@NRGA are shown in Fig. S1 in the Supplementary Material. The NRGA mass density was estimated to be around 0.0110 g/cm^3. The density increased to about 0.0187 g/cm^3 after the addition of the Ni-NPs, implying that the addition of the Ni-NPs suppresses the lightweight feature of the NRGA. The mass density of Ni-SA@NRGA, on the other hand, is reduced to 0.0141 g/cm^3, which is slightly higher than that of the pure NRGA. As a result, anchoring the Ni-SAs has little effect on the NRGA's lightweight feature. Ni contents in Ni-SA@NRGA and Ni-NP@NRGA are approximately 3.36 and 46.91 wt%, respectively, as determined by inductively coupled plasma-optical emission spectrometry (ICP-OES). Images from scanning electron microscopy (SEM) and transmission electron microscope (TEM) show that N-doped graphene (NG) has a curly sheet-like morphology [Figs. S3(a) and S3(b)]. Micropores can be seen in the graphene sheets, which aid in the anchoring of the M-SAs. The TEM images and element mappings show the coexistence of C, N, and O atoms in the NRGA [Fig. S3(d)], demonstrating N doping into graphene.[15] The surface oxygen-containing functional groups are responsible for the O signals. Ni-NP@NRGA SEM images [Fig. S4(a)] show that some large nanoparticles (50–300 nm) are distributed on the graphene sheet or wrapped by the graphene layer. The nanoparticles are metal Ni particles according to the TEM images and element mappings. Moreover, the Ni signals are also observed in the region without Ni nanoparticles, suggesting that the Ni-SAs are formed and anchored on the NG. Furthermore, the C, N, and O signals are observed, indicating that, in addition to Ni nanoparticles, surface oxygen-containing functional groups existed in the Ni-NP@NRGA.

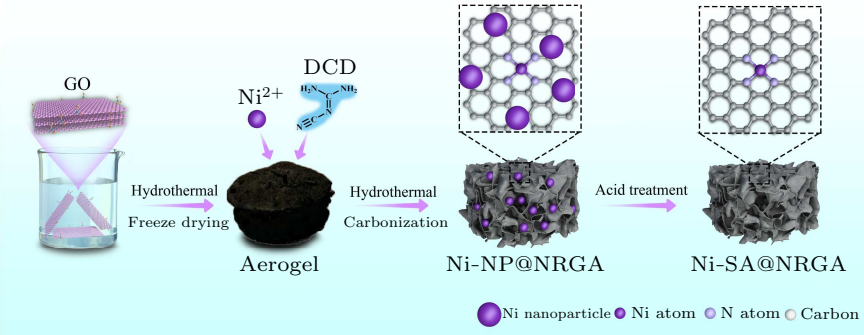

Fig. 1. Schematic illustration of the fabrication process of the Ni-SA@NRGA.

The Ni-SA@NRGA SEM image demonstrates that the NRGA's sheet-like morphology has been preserved [Fig. 2(a)]. The SEM image of Ni-SA@NRGA (Fig. S2) reveals that the aerogel is porous, with an average pore size of 13 μm. The inset of Fig. 2(a) shows that the Ni-SA@NRGA can be supported by Setaria Viridis, confirming its ultralight nature. The TEM images [Figs. 2(b) and 2(c)] show that metallic nanoparticles and clusters are missing from the Ni-SA@NRGA, indicating that the Ni nanoparticles were completely removed during the acid etching process. In addition, micropores can be found in the N-doped sheets. The aberration-corrected high-angle annular dark-field scanning transmission electron microscopy

(AC-HAADF-STEM) image shows that some bright spots are evenly distributed on the NG, which correspond to the heavy Ni single atoms [Fig. 2(d)].[16]

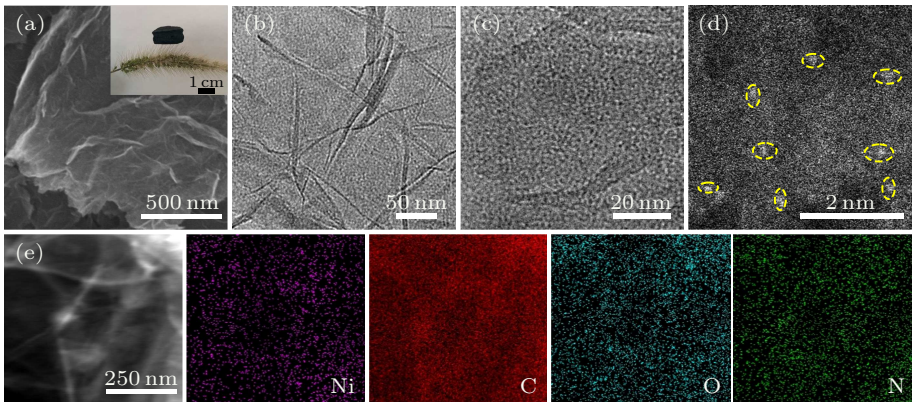

Fig. 2. (a) SEM image of the Ni-SA@NRGA, with the inset showing the digital photograph of Ni-SA@NRGA on the Setaria Viridis. (b) TEM image of the Ni-SA@NRGA. (c) HRTEM image of the Ni-SA@NRGA. (d) AC-HAADF-STEM image of the Ni-SA@NRGA. (e) TEM image and the corresponding EDX Ni, C, O, and N mappings of Ni-SA@NRGA.

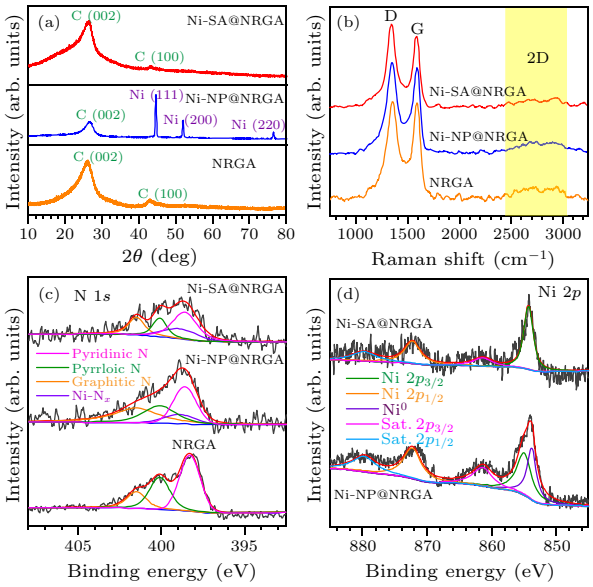

Fig. 3. (a) XRD patterns and (b) Raman spectra of Ni-SA@NRGA, Ni-NP@NRGA, and NRGA. (c) XPS spectra of N 1*s* of NRGA, Ni-SA@NRGA, and Ni-NP@NRGA. (d) XPS spectra of Ni 2*p* of Ni-SA@NRGA and Ni-NP@NRGA.

To further characterize the crystal structure and composition of the sample, Fig. 3(a) shows the x-ray diffraction (XRD) patterns of the samples. Two diffraction peaks at 26.3° and 43.0° in the NRGA and Ni-SA@NRGA XRD patterns correspond to the (002) and (100) planes of graphitic carbon (JCPDS card No. 41-1487), respectively.[17] The diffraction peaks of the Ni metals are not shown, revealing the absence of the Ni nanoparticles or clusters in two samples. The XRD pattern of Ni-NP@NRGA, on the other hand, shows diffraction peaks at 44.5°, 51.8°, and 76.3°, which can be indexed to (111), (200), and (220) planes of cubic Ni (JCPDS card No. 04-0850), respectively.[18] Figure 3(b) shows the Raman spectra of Ni-SA@NRGA, Ni-NP@NRGA, and NRGA. In the Raman spectra, the two peaks of carbon-based materials at 1351 and 1591 cm^{-1} correspond to the D-band and G-band, respectively.[19] The intensity ratios (I_D/I_G) of Ni-SA@NRGA, Ni-NP@NRGA, and NRGA are 1.17, 1.06, and 1.03, respectively, indicating that Ni-SA@NRGA has the least degree of graphitization with abundant edge defects. Furthermore, 2D peaks of aerogels can be found in Raman spectra, indicating graphene multilayer properties.[20] X-ray photoelectron spectroscopy (XPS) shows the presence of Ni, C, N, and O elements in Ni-SA@NRGA and Ni-NP@NRGA, while C, N, and O elements in NRGA (Fig. S6). Three typical characteristic peaks of high-resolution C 1*s* XPS spectra of Ni-SA@NRGA, Ni-NP@NRGA, and NRGA located at 284.6, 285.1, and 286.2 eV correspond to the C–C, C–N, and C–O/C=O groups in Fig. S5, respectively.[4] The N 1*s* XPS spectra of Ni-SA@NRGA and Ni-NP@NRGA are shown in Fig. 3(c), with binding energies centered at 401.5, 398.9, 400.1, and 398.6 eV, which could correspond to graphitic-N, Ni-N_x, pyrrolic-N, and pyridinic-N, respectively.[4,21] In contrast, the Ni-N_x species are not detected in the NRGA XPS spectra, implying that no Ni-SAs are present in the sample (Fig. S6). The high-resolution Ni 2*p* XPS spectrum of Ni-SA@NRGA, as shown in Fig. 3(d), shows two peaks at about 854.3 eV (Ni $2p_{3/2}$) and 872.3 eV (Ni $2p_{1/2}$), which can be attributed to the Ni-N_x species, with satellite peaks at 861.4 and 879.8 eV.[21,22] There are no metallic nickel signals observed, indicating that the Ni species are primarily anchored on the NG in the form of SAs. In contrast, metallic Ni with a binding energy of 853.8 eV was detected in the Ni 2*p* XPS spectra of Ni-NP@NRGA, in addition to the Ni-N_x species [Fig. 3(d)].[23] The binding energies of the Ni-N_x in the Ni-NP@NRGA shift negatively when compared to

the Ni-SA@NRGA, indicating an electronic interaction between metallic Ni nanoparticles and Ni-N_x. A sample vibration magnetometer was used to measure the magnetic properties of the Ni-SA@NRGA and Ni-NP@NRGA. The magnetization hysteresis loops show that Ni-NP@NRGA with Ni particles is ferromagnetic, whereas Ni-SA@NRGA with Ni single atoms is diamagnetism, confirming the complete removal of Ni-NPs in the Ni-SA@NRGA sample (Fig. S7).[24,25]

The EM parameters of samples with a filler ratio of 25 wt% in the paraffin matrix were determined. The reflection loss (R_L) and the effective absorbance (EAB) are important criteria for evaluating the absorbing performance of the samples. Based on the transmission line theory, the R_L was calculated based on the measured electromagnetic parameters [Eqs. (S1) and (S2) in Supporting Information].[26–28] The NRGA's $R_{L,min}$ was only −30.12 dB at a thickness of d = 5.0 mm, and its EAB is only 2.0 GHz with d = 2.5 mm, indicating poor absorption performance [Fig. S8(a)]. The absorption property was improved significantly after the addition of Ni nanoparticles. The minimum R_L value of Ni-NP@NRGA is −40.53 dB at 4.72 GHz with d = 4.5 mm, and the largest EAB is increased to 2.24 GHz with d = 2.5 mm, as shown in Fig. 4(a). If the Ni nanoparticles were removed, the absorption property was further improved. As illustrated in Fig. 4(b), the $R_{L,min}$ value of Ni-SA@NRGA is −49.46 dB with d = 2.0 mm, and its largest EAB is 3.12 GHz with a small d = 1.5 mm. Furthermore, when d is within the scope of 1.5–5.0 mm, the $R_{L,min}$ values of Ni-SA@NRGA exceed −10 dB. Furthermore, even if the matching thickness is in the range of 1.2–2.0 mm, the $R_{L,min}$ value of Ni-SA@NRGA can exceed above −20 dB [Fig. 4(c)]. As a result, Ni-SA@NRGA has better EMW absorption performance than that of the NRGA and the Ni-NP@NRGA, demonstrating that the incorporation of Ni-SAs into the NRGA is beneficial to improving the EWA performance. Furthermore, in terms of thickness or filler ratio, the absorption property of the Ni-SA@NRGA is comparable or superior to the magnetic carbon-based absorbers, implying that it has promising applications in the EWA field (Table S1).[29–32]

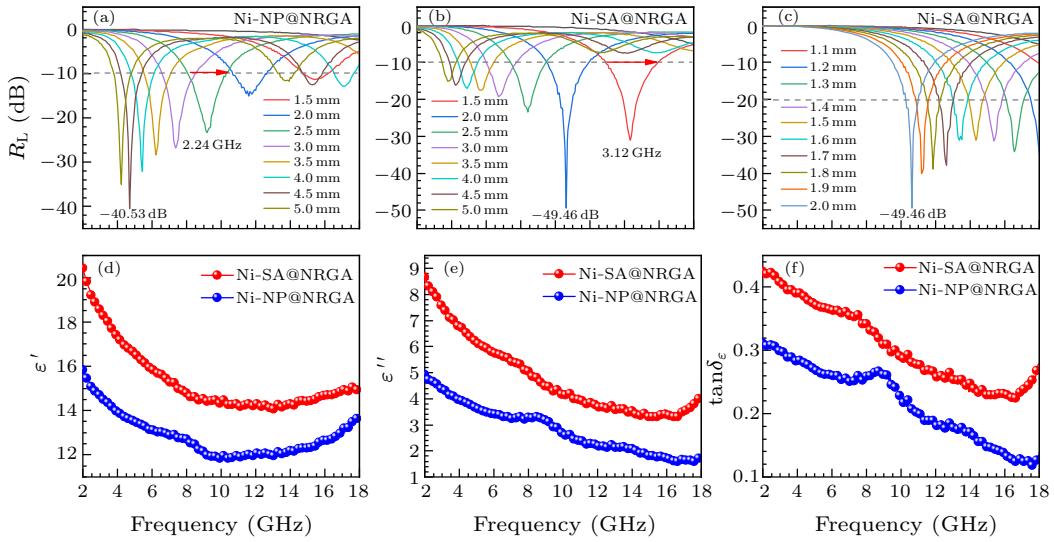

Fig. 4. (a) R_L–f curves of Ni-NP@NRGA with thickness of 1.5–5.0 mm. (b) R_L–f curves of Ni-SA@NRGA with thickness of 1.5–5.0 mm. (c) R_L–f curves of Ni-SA@NRGA with thickness of 1.1–2.0 mm. (d)–(f) Behaviors of ε', ε'' and $\tan\delta_\varepsilon$ of the complex permittivity and loss tangents of the Ni-SA@NRGA and Ni-NP@NRGA samples.

The electromagnetic parameters of Ni-SA@NRGA and Ni-NP@NRGA are compared for determining the reasons of the enhanced electromagnetic absorption performance of Ni-SA@NRGA. The real parts (ε') of the complex permittivity of Ni-SA@NRGA and Ni-NP@NRGA as a function of frequency are shown in Fig. 4(d). The ε' values of the samples gradually decrease with increasing frequency in the low-frequency region ($\lesssim$10 GHz), and then slightly rise in the high-frequency region, which may be due to the enhancement of the polarization relaxations in the high-frequency region.[33] Over 2–18 GHz, the ε' values of Ni-SA@NRGA (14.07– 20.41) are significantly higher than those of Ni-NP@NRGA (11.81–15.83). Simultaneously, as shown in Fig. 4(e), the imaginary parts (ε'') of the complex permittivity of Ni-SA@NRGA are changed in the range of 3.28–8.67, which is larger than that of Ni-NP@NRGA (1.59–4.93). The larger ε' and ε'' values of the Ni-SA@NRGA imply that it has better EMW energy and attenuation abilities. Furthermore, the dielectric loss tangent ($\tan\delta_\varepsilon = \varepsilon''/\varepsilon'$) of the Ni-SA@NRGA varies in the range of 0.22–0.42, which is greater than that of the Ni-NP@NRGA (0.11–0.35), indicating that the Ni-SA@NRGA has improved

dielectric loss performance over the Ni-NP@NRGA [Fig. 4(f)]. As a result, the improved absorption property of Ni-SA@NRGA can be attributed to its increased dielectric loss. Furthermore, the ε' and ε'' values of the NRGA are lower than those of Ni-SA@NRGA [Figs. S8(b) and S8(c)]. As a result, the NRGA has lower $\tan\delta_\varepsilon$ values [Fig. S9(c)], leading to its inferior EWA property to that of Ni-SA@NRGA.

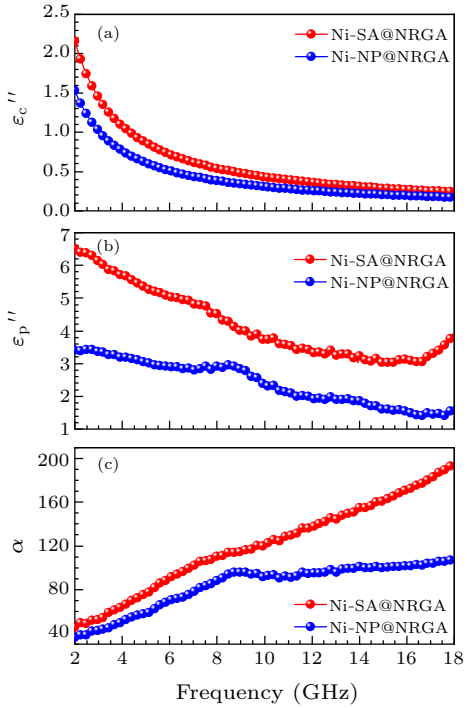

Fig. 5. (a) Conductive loss and (b) polarization loss of Ni-SA@NRGA and Ni-NP@NRGA. (c) The attenuation coefficients of Ni-SA@NRGA and Ni-NP@NRGA.

To understand the difference in dielectric loss between the samples, the sources of ε'' of the samples were analyzed. In general, ε'' of a dielectric material includes conduction loss (ε_c'') and polarization relaxation loss (ε_p'').[21] The straight line and the semicircle in the Cole–Cole plots indicate that the three samples have both conduction and polarization relaxation losses (Fig. S11).[34] The measured σ values by an electrochemical station in a low-frequency range were 0.24, 0.17, and 0.14 S m^{-1} for Ni-SA@NRGA, Ni-NP@NRGA, and NRGA, respectively. According to the values, ε_c'' values of the samples were estimated. The conductivity losses of Ni-SA@NRGA are higher than those of Ni-NP@NRGA and NRGA, as shown in Figs. 5(a) and S9(a), especially at low frequencies. Meanwhile, the ε_p'' values of Ni-SA@NRGA are also much higher than those of Ni-NP@NRGA and NRGA [Figs. 5(b) and S9(b)]. As previously reported, the introduction of M-SAs into a nanocarbon matrix regulates the electronic structure of the adjacent carbon atoms, increasing the electrical conductivity of the nanocarbon containing M-SAs.[14] As a result, the increased conduction loss of the Ni-SA@NRGA is understandable. Meanwhile, polarization systems would be created by combining M-SAs with nanocarbons, causing charge transfer due to the different electronegativities of the metal, nitrogen, and carbon atoms. The interaction of the M-SAs-containing nanocarbons with EMW could induce polarization loss in the formed polarization systems, increasing the polarization loss.[14,35] As a result, the improved dielectric loss performance of the Ni-SA@NRGA is attributed to increases in both ε_c'' and ε_p'', which are greater than those of Ni-NP@NRGA and NRGA.

Figure S10 shows the comparison of relatively complex permeability for the three samples. It is found that the $\tan\delta_\mu = \mu''/\mu'$ values (μ' and μ'' are real and imaginary parts of the complex permeability, respectively) are less than 0.13, indicating that magnetic loss is not a significant factor in the EWA properties of the three samples. Aside from dielectric and magnetic losses, absorbers impedance matching characteristic is also an important factor in its EWA property. To assess the degree of impedance matching, one can use the impedance characteristic $|Z| = |Z_{in}/Z_0|$ [Eq. (S3)]. If $|Z|$ is infinitely close to 1, the absorber has the best impedance matching characteristic, making it easier to improve EWA.[36] The $|Z|$–f plots of Ni-SA@NRGA, Ni-NP@NRGA, and NRGA are shown in Figs. S12(a)–S12(c). When d is in the range 1.5–2.0 mm, the $|Z|$ values of Ni-SA@NRGA are closer to 1 compared to Ni-NP@NRGA and NRGA. Thus, the improved EWA property of the Ni-SA@NRGA is related to its improved impedance matching performance.

In addition to the EWA property, an absorber's attenuation ability is critical for its practical application. The attenuation coefficient α can be used to evaluate an absorber's attenuation ability [Eq. (S4)].[37] As shown in Fig. 5(c), the α values of Ni-SA@NRGA vary in the range 49.8–181.1 over 2–18 GHz, which is higher than the values of Ni-NP@NRGA (35.9–109.1) and NRGA (33.3–115.2), indicating that Ni-SA@NRGA has better attenuation ability toward the EMW. The strong EWA property and attenuation ability of Ni-SA@NRGA are a potential candidate for the EWA field.[38,39]

In summary, we have used a simple method to create ultralight NG aerogels with anchoring uniform dispersion of nickel single atoms (Ni-SA@NRGA). As lightweight EMW absorbers, the Ni-SA@NRGA exhibits outstanding EWA performance with a minimum R_L of −49.46 dB and a thickness of only 2.0 mm, and its largest EAB is up to 3.12 GHz (below −10 dB). The results indicate that introduction of Ni-SAs and coordinated with nitrogen species (M-N$_x$) immobilized on carbon matrix can raise dielectric loss aroused by conductive loss, polarization relaxation. Furthermore, the multiple scattering of the Ni-SA@NRGA porous

structure improves EWA performance, outperforming most reported carbon-based EMW absorbing materials. As a result, it is thought that this work provides new ideas and methods for a new pattern of EWA materials with higher R_{L}, a wider absorption frequency boundary, and lighter weight.

Acknowledgements. This work was supported by the National Natural Science Foundation of China (Grant No. 51972077), the Heilongjiang Touyan Innovation Team Program, and the Fundamental Research Funds for the Central Universities (Grant Nos. 3072020CF2518, 3072020CFT2505, and 3072020CFJ2503).

References

[1] Zhao H Q, Cheng Y, Zhang Z, Zhang B S, Pei C C, Fan F Y and Ji G B 2021 *Carbon* **173** 501
[2] Zhu X, Yan F, Li C Y, Qi L H, Yuan H R, Liu Y F, Zhu C L and Chen Y J 2021 *Chin. Phys. Lett.* **38** 015201
[3] Wang Z C, Wei R B, Gu J W, Liu H, Liu C T, Luo C J, Kong J, Shao Q, Wang N, Guo Z H and Liu X B 2018 *Carbon* **139** 1126
[4] Zhang X C, Xu J, Yuan H R, Zhang S, Ouyang Q Y, Zhu C L, Zhang X T and Chen Y J 2019 *ACS Appl. Mater. Interfaces* **11** 39100
[5] Che R C, Peng L M, Duan X F, Chen Q and Liang X L 2004 *Adv. Mater.* **16** 401
[6] Sun H, Che R C, You X, Jiang Y S, Yang Z B, Deng J, Qiu L B and Peng H S 2014 *Adv. Mater.* **26** 8120
[7] Liu Q H, Cao Q, Bi H, Liang C Y, Yuan K P, She W, Yang Y J and Che R C 2016 *Adv. Mater.* **28** 486
[8] Zhang X, Yan F, Zhang S, Yuan H R, Zhu C L, Zhang X T and Chen Y J 2018 *ACS Appl. Mater. Interfaces* **10** 24920
[9] Sultanov F, Daulbayev C, Bakbolat B and Daulbayev O 2020 *Adv. Colloid Interface Sci.* **285** 102281
[10] Zhi D D, Li T, Li J Z, Ren H S and Meng F B 2021 *Compos. Part. B: Eng.* **211** 108642
[11] Hu C G, Mou Z Y, Lu G W, Chen N, Dong Z L, Hu M J and Qu L T 2013 *Phys. Chem. Chem. Phys.* **15** 13038
[12] Ren S, Yu Q, Yu X H, Rong P, Jiang L Y and Jiang J C 2020 *Sci. China Mater.* **63** 903
[13] Zhang L L, Liu D B, Muhammad Z, Wan F, Xie W, Wang Y J, Song L, Niu Z Q and Chen J 2019 *Adv. Mater.* **31** 1903955
[14] Zhang X C, Shi Y N, Xu J, Ouyang Q Y, Zhang X, Zhu C L, Zhang X L and Chen Y J 2022 *Nano-Micro Lett.* **14** 27
[15] Wu L Z, Shu R W, Zhang J B and Chen X T 2022 *J. Colloid Interface Sci.* **608** 1212
[16] Cheng Y, Zhao S Y, Li H B, He S, Veder J P, Johannessen B, Xiao J P, Lu S F, Pan J, Chisholm M F, Yang S Z, Liu C, Chen J G and Jiang S P 2019 *Appl. Catal. B: Environ.* **243** 294
[17] Zhao H B, Cheng J B, Zhu J Y and Wang Y Z 2019 *J. Mater. Chem. C* **7** 441
[18] Cao F H, Yan F, Xu J, Zhu C L, Qi L H, Li C Y and Chen Y J 2021 *Carbon* **174** 79
[19] Huang X G, Yu G Y, Zhang Y K, Zhang M J and Shao G F 2021 *Chem. Eng. J.* **426** 131894
[20] Zhang K C, Gao X B, Zhang Q, Li T P, Chen H and Chen X F 2017 *J. Alloys Compd.* **721** 268
[21] Xu J, Zhang X, Zhao Z B, Yuan H R, Zhang S, Zhu C L, Zhang X T and Chen Y J 2020 *Carbon* **159** 357
[22] Yuan C Z, Zhan L Y, Liu S J, Chen F, Lin H J, Wu X L and Chen J R 2020 *Inorg. Chem. Front.* **7** 1719
[23] Zhang X C, Zhang X, Yuan H R, Li K Y, Ouyang Q Y, Zhu C L, Zhang S and Chen Y J 2020 *Chem. Eng. J.* **383** 123208
[24] Pandey R, Tekumalla S and Gupta M 2019 *J. Alloys Compd.* **770** 473
[25] Xu D W, Yang S, Chen P, Yu Q, Xiong X H and Wang J 2019 *Carbon* **146** 301
[26] Liu J W, Che R C, Chen H J, Zhang F, Xia F, Wu Q S and Wang M 2012 *Small* **8** 1214
[27] Che R C, Zhi C Y, Liang C Y and Zhou X G 2006 *Appl. Phys. Lett.* **88** 033105
[28] Wu Z C, Pei K, Xing L S, Yu X F, You W B and Che R C 2019 *Adv. Funct. Mater.* **29** 1901448
[29] Huang Y W, Wang Y J, Wei S C, Liang Y, Huang W, Wang B and Xu B S 2019 *Int. J. Mod. Phys. B* **33** 1940055
[30] Chen T T, Deng F, Zhu J, Chen C F, Sun G B, Ma S L and Yang X J 2012 *J. Mater. Chem.* **22** 15190
[31] Ma T, Yuan M W, Islam S M, Li H F, Ma S L, Sun G B and Yang X J 2016 *J. Alloys Compd.* **678** 468
[32] Yin P F, Deng Y, Zhang L M, Wu W J, Wang J, Feng X, Sun X Y, Li H Y and Tao Y 2018 *Ceram. Int.* **44** 20896
[33] Wang D T, Wang X C, Zhang X, Yuan H R and Chen Y J 2020 *Chin. Phys. Lett.* **37** 045201
[34] Tang J M, Liang N, Wang L, Li J, Tian G, Zhang D, Feng S H and Yue H J 2019 *Carbon* **152** 575
[35] Xu J, Liu M J, Zhang X C, Li B, Zhang X, Zhang X L, Zhu C L and Chen Y J 2022 *Appl. Phys. Rev.* **9** 011402
[36] Chen J P, Jia H, Liu Z, Kong Q Q, Hou Z H, Xie L J, Sun G H, Zhang S C and Chen C M 2020 *Carbon* **164** 59
[37] Liu B, Li J H, Wang L F, Ren J H and Xu Y F 2017 *Compos. Part. A: Appl. Sci. Manuf.* **97** 141
[38] Cai Z X, Su L, Wang H J, Niu M, Gao H F, Lu D and Li M Z 2020 *ACS Appl. Mater. Interfaces* **12** 8555
[39] Cai Z X, Su L, Wang H J, Niu M, Tao L T, Lu D, Xu L, Li M Z and Gao H F 2021 *ACS Appl. Mater. Interfaces* **13** 16704

Supplementary Material: Atomically dispersed Ni single-atoms anchored on N-doped graphene aerogels for highly efficient electromagnetic wave absorption

Bing Suo , Xiao Zhang*, Xinyu Jiang, Feng Yan*, Zhengzhi Luo, Yujin Chen*

Key Laboratory of In-Fiber Integrated Optics, Ministry of Education and College of Physics and Optoelectronic Engineering, Harbin Engineering University, Harbin 150001, China. E-mail address: chenyujin@hrbeu.edu.cn.

EXPERIMETNAL SECTION

Materials. Graphene oxide (GO) was purchased from Shenzhen Yuechuang Evolution Technology Co., Ltd., nickel chloride hexahydrate ($NiCl_2$ $6H_2O$), dicyandiamide (DCD), and ethanol (C_2H_5OH) were purchased from Tianjin Guangfu Fine Chemical Research Institute (China). All chemicals were used directly without further purification.

Synthesis of NRGA. Graphene oxide (GO) (50 mg) was dispersed in water (10 mL) under the sonication for 30 min. Then the suspension was transferred into a Teflon-lined stainless-steel autoclave, and hydrothermally treated at 180 ℃ for 10 hours. The prepared hydrogel was freeze-dried for 24 hours. The obtained aerogel was immersed in the 25 mL of ethanol containing 0.35 g of dicyandiamide, and then hydrothermally treated at 180 ℃ for 2 hours. Finally, the GA was heated at 900 ℃ for 2 hours under argon atmosphere to obtain NRGA.

Synthesis of Ni-NP@NRGA. GO (50 mg) was dispersed in water (10 mL) under the sonication for approximately 30 min. Then the suspension was transferred into a Teflon-lined stainless-steel autoclave, and hydrothermally treated at 180 ℃ for 10 hours. The prepared hydrogel was freeze-dried for 24 hours. The obtained aerogel was immersed in 50 mL ethanol/water (v:v = 1:1) containing 0.7 g of nickel chloride hexahydrate and 0.35 g of dicyandiamide, and then hydrothermally treated at 180 ℃ for 2 hours. Finally, the GA was heated at 900 ℃ for 2 hours under flowing argon to

obtain Ni-NP@NRGA.

Synthesis of Ni-SA@NRGA. The obtained Ni-NP@NRGA was treated 2 M H_2SO_4 solution at 80℃ for 12 h to remove the Ni nanoparticles.

Characterizations. The morphology, size and structure of all samples was observed using a Hitachi SU8000 scanning electron microscope (SEM) at an accelerating voltage of 15 kV and the test current of 10 μA. The sample was mixed with ethanol under ultrasonic to uniform dispersion, after that drop dispersion solution onto the copper sheet which fixed with conductive tape, then placed into the cavity mirror for observation. The refined structure, crystallization, morphology, particle size and composition of the material were characterized by Hitachi JEM-2100 transmission electron microscope operating at a voltage of 200 kV. The sample was mixed with ethanol by ultrasonic until it was evenly dispersed before the test, and then dropped dispersion solution onto the micro-grid and observed under the endoscope. The crystal structure and composition of the synthesized samples were characterized by X-ray powder diffraction (XRD) using a X Pert Pro diffractometer with Cu Kα radiation (λ=1.5418 Å) in the scattering range (2θ) of 15–90° with a scanning rate of 5°/min. The surface chemical compositions and valence states were qualitative analyzed by X-ray photoelectron spectroscopy (XPS, K-Alpha, Thermofisher Scienticfic Company). Raman spectra was used to characterize the disorder degree of carbon materials and acquired at room temperature by Lab RAM Aramis micro Raman spectrometer in the range of 500–2500 cm^{-1} with an excitation wavelength at 488 nm. The magnetic properties of samples were measured using a vibrating sample magnetometer (VSM; Lakeshore 7404) at room temperature. Mentallic elemental content of the samples was analyzed by inductively coupled plasma-optical emission spectroscopy (ICP-OES) were tested by iCPA 7000 Series spectrometer.

Electromagnetic parameter measurement. The microwave absorption properties and electromagnetic parameters of the absorbing materials were measured by using a vector network analyzer (Anritsu MS4644A Vectorstar) in the range of 2–18 GHz at the room temperature. The absorbing materials (25 wt%) to be tested is mixed with paraffin wax, and a specific abrasive tool is used to form a ring (ring inner diameter

3.04 mm, outer diameter 7.0 mm, thickness about 2.5 mm), and then the electromagnetic parameters of the sample are measured by the coaxial transmission/reflection method.

The reflection loss is used to evaluate the electromagnetic wave absorption ability of the material through the reflection loss R_L (Reflection loss) (dB) of the material to the electromagnetic wave. According to transmission line theory, the formula for reflection loss is as follows:

$$Z_{in} = Z_0\sqrt{\frac{\mu_r}{\varepsilon_r}}\tanh\left(j\frac{2\pi fd\sqrt{\mu_r\varepsilon_r}}{c}\right) \quad \text{(S1)}$$

$$R_L(dB) = 20log_{10}\left|\frac{Z_{in}-Z_0}{Z_{in}+Z_0}\right| \quad \text{(S2)}$$

Among them, Z_{in}, Z_0, ε_r, μ_r are the input impedance of the absorbing material, the inherent impedance of air, the relative complex permittivity and the permeability, respectively; where c, f, and d are the speed of light, electromagnetic wave frequency andcoating layer thickness, respectively.[1]

The impedance matching characteristic can be estimated the extent of impedance matching, where $|Z|$ is the normalized impedance[2], its expression is as follows:

$$|Z| = |Z_{in}/Z_0| \quad \text{(S3)}$$

For the attenuation condition, in order to make the attenuation ability of materials to electromagnetic waves better, the material often needs to have a large attenuation coefficient α, which is often used to measure the attenuation ability of materials to electromagnetic waves, its expression is as follows:

$$\alpha = \frac{\sqrt{2\pi f}}{c}\sqrt{(\mu''\varepsilon''-\mu'\varepsilon')+\sqrt{(\mu''\varepsilon''-\mu'\varepsilon')^2+(\mu'\varepsilon''+\mu''\varepsilon')^2}} \quad \text{(S4)}$$

In formula (S3), ε' and ε'' represent the real and imaginary parts of the material's complex permittivity, respectively; μ' and μ'' respectively represent the real and imaginary parts of the complex permeability.[3]

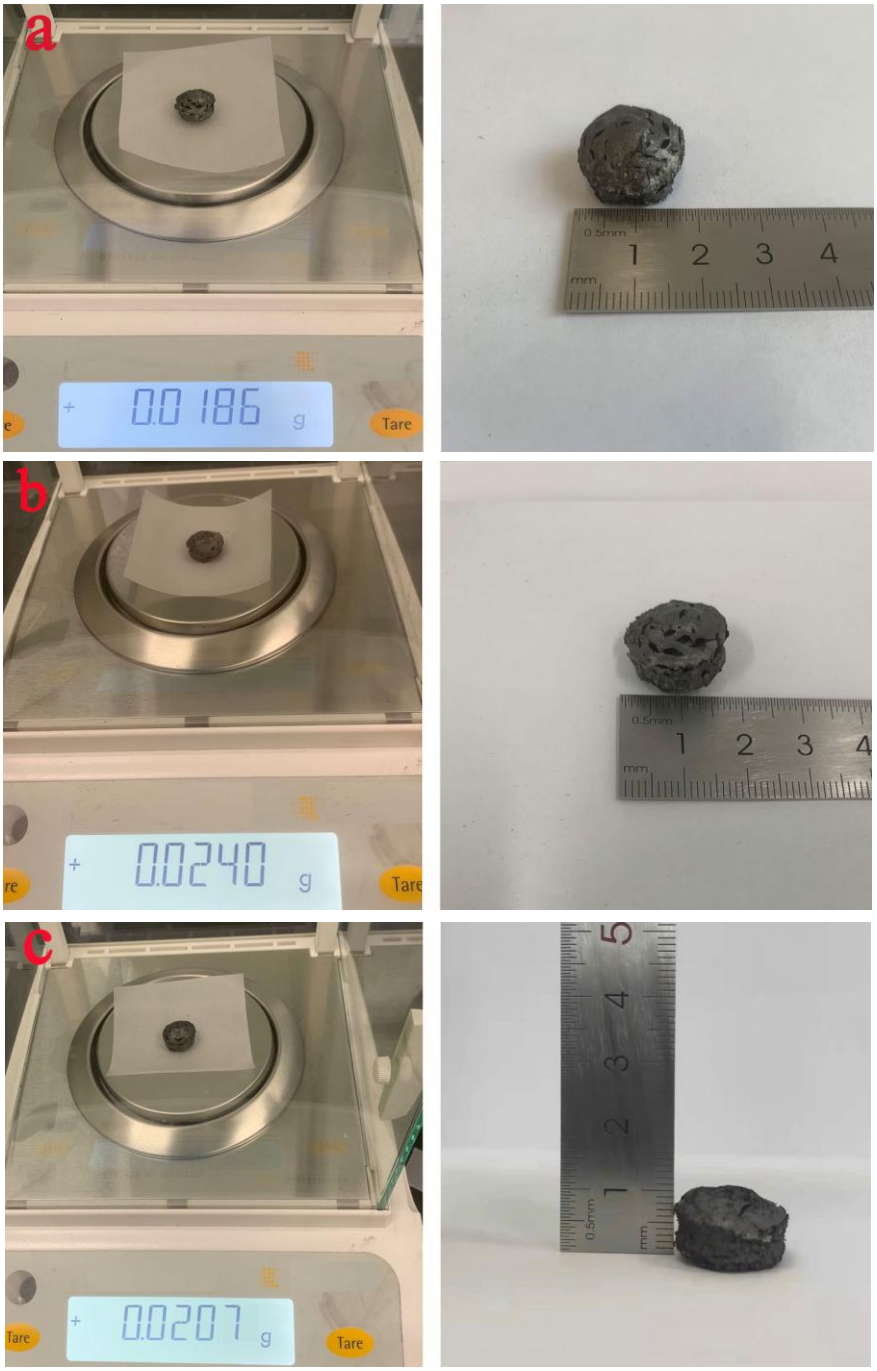

FIG. S1:The digital photographs of (a) NRGA , (b) Ni-NP@NRGA and (c) Ni-SA@NRGA.

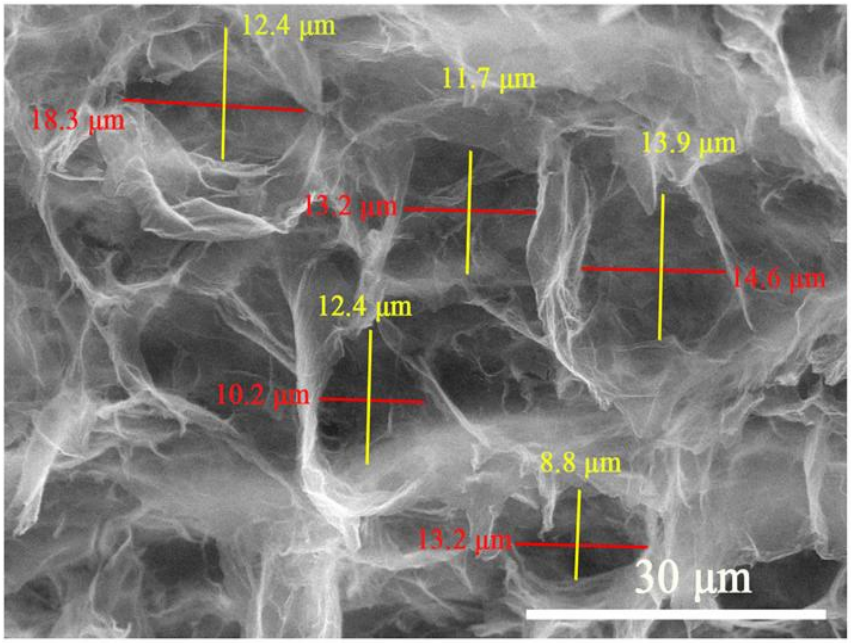

FIG. S2: SEM image of Ni-SA@NRGA.

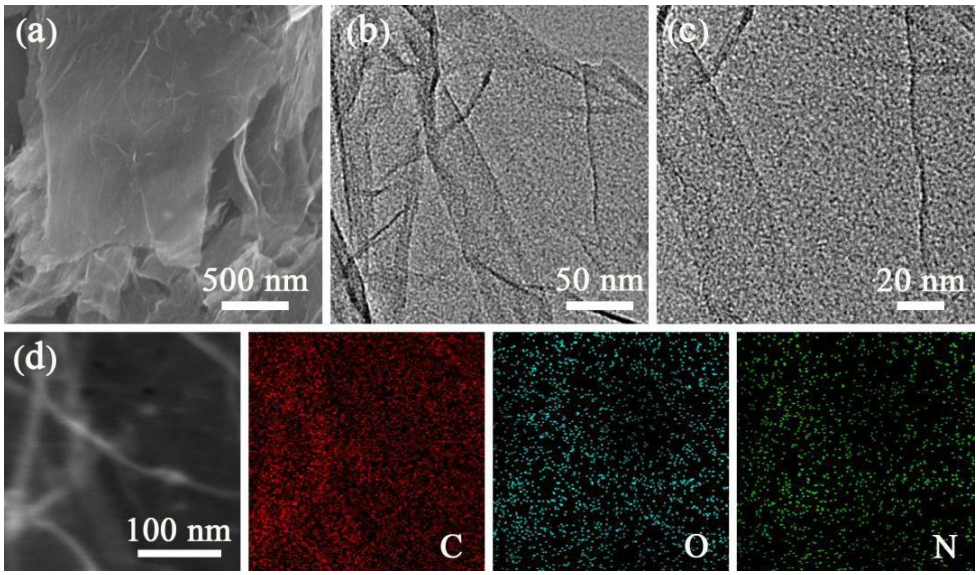

FIG. S3: (a) SEM image of NRGA. (b) TEM images of the NRGA. (c) HRTEM images of the NRGA. (d) TEM image and the corresponding EDX C, N and O mappings of NRGA.

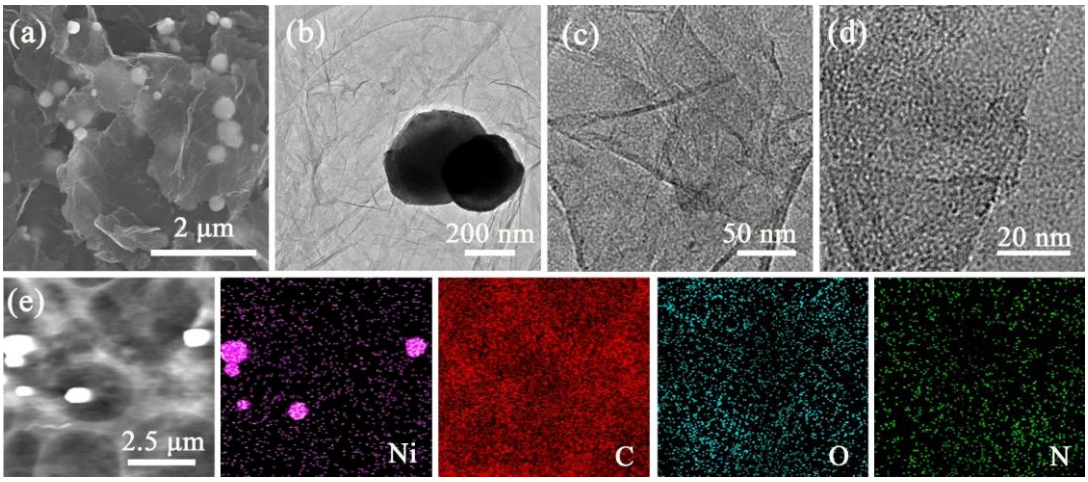

FIG. S4: (a) SEM images of the Ni-NP@NRGA. (b) TEM images of the Ni-NP@NRGA. (c) HRTEM images of the Ni-NP@NRGA. (d) TEM image and the corresponding EDX Ni, C, N and O mappings of Ni-NP@NRGA.

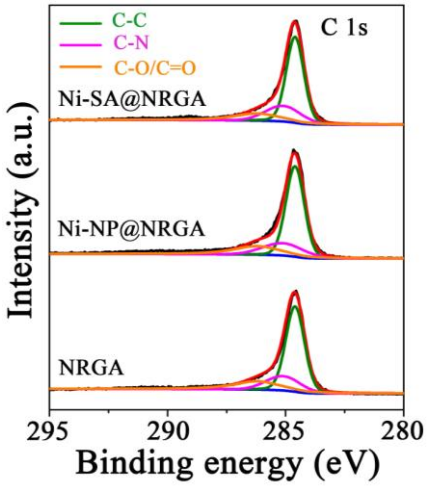

FIG. S5: XPS spectra of C 1s of Ni-SA@NRGA , Ni-NP@NRGA and NRGA.

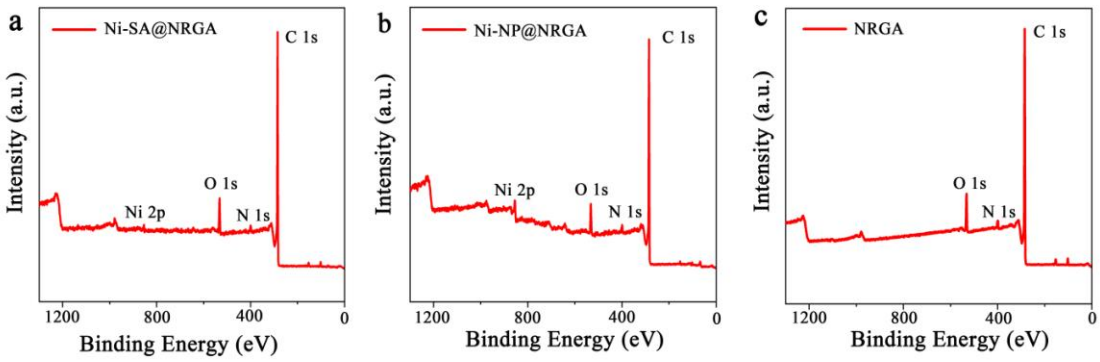

FIG. S6: XPS survey spectra of the (a) Ni-SA@NRGA, (b) Ni-NP@NRGA and (c) NRGA.

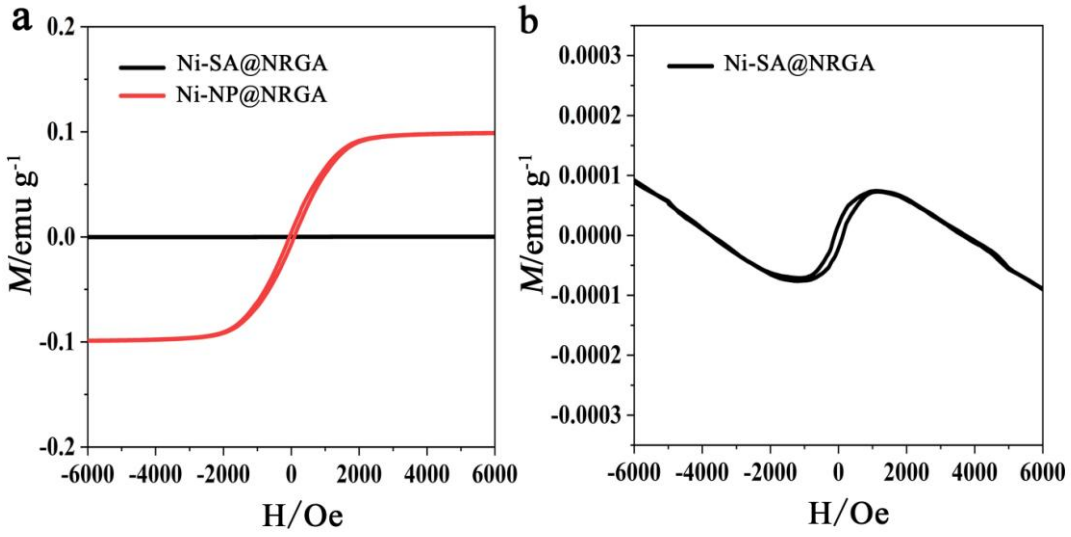

FIG. S7: The magnetic hysteresis loops of the (a) Ni-SA@NRGA and Ni-NP@NRGA, (b) an enlarged image of the Ni-SA@NRGA

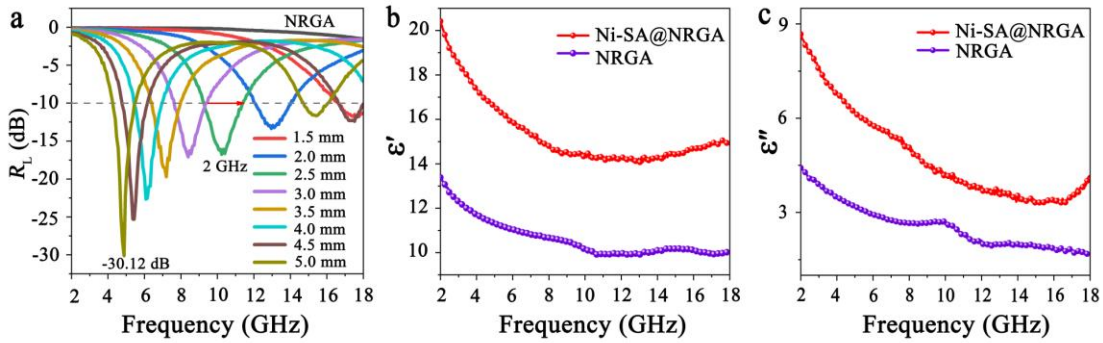

FIG. S8: (a) The reflection loss (R_L) of NRGA at d in range of 1.5mm-5.0mm. (b)-(c)The real part (ε') , the imaginary part (ε'') value of the complex permittivity of the Ni-SA@NRGA and NRGA.

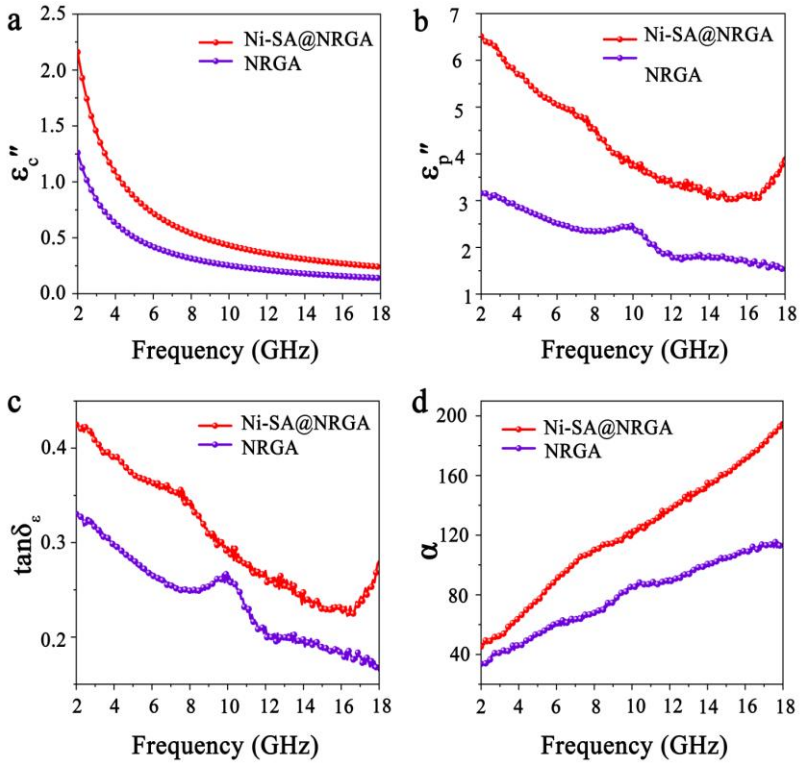

FIG. S9: (a) Conductive loss and (b) polarization loss of Ni-SA@NRGA and NRGA. (c) The dielectricloss tangents of the Ni-SA@NRGA and NRGA. (d) The attenuation coefficient α of Ni-SA@NRGA and NRGA.

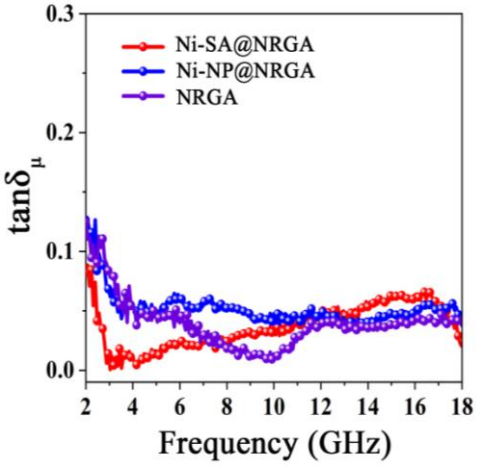

FIG. S10: The magnetic loss tangent of the Ni-SA@NRGA, Ni-NP@NRGA and NRGA.

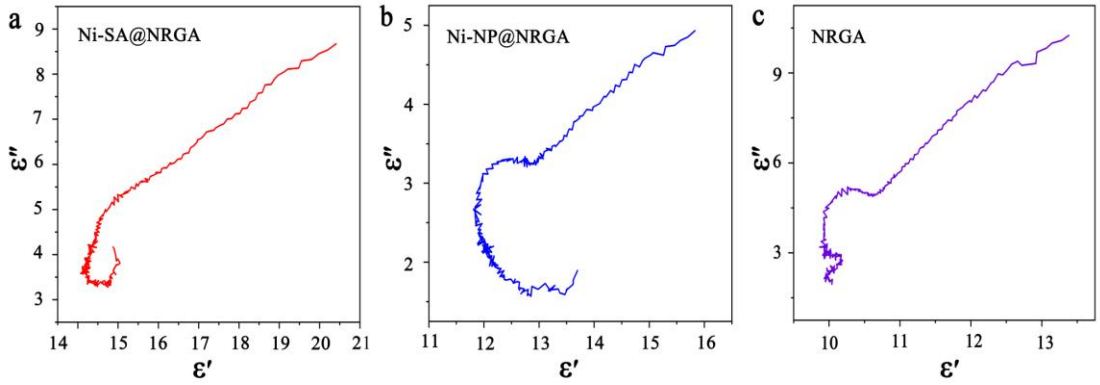

FIG. S11: ε′-ε" plots of (a) Ni-SA@NRGA, (b) Ni-NP@NRGA and (c) NRGA.

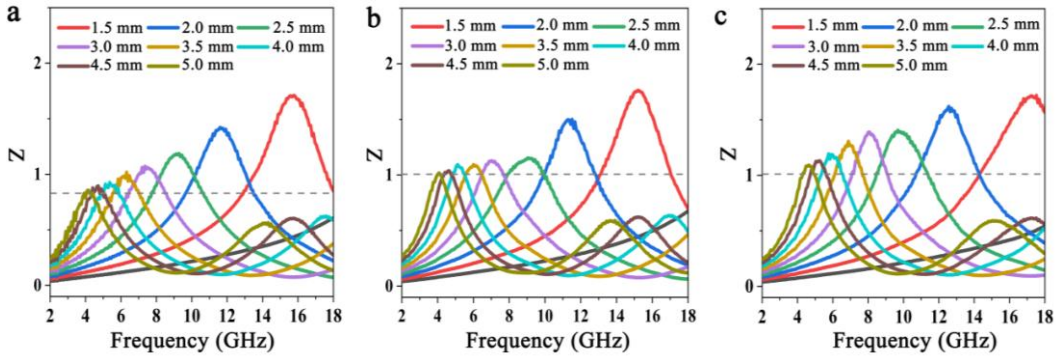

FIG. S12: The impedance coefficient |*Z*| of the (a) Ni-SA@NRGA, (b) Ni-NP@NRGA and (c) NRGA.

Table S1. EMW Absorption Properties of 3D Ni-SA@NRGA and Other Reported Carbon-based Absorbers

Absorbers	R_{Lmin} (dB)	Thinkness (mm)	Filler Ratio (wt%)	Ref.
GO/CNT-Fe_3O_4	-28.57	2.00	30	4
Graphene/Fe_3O_4/Ni composites	-16.38	3.50	60	5
CF-RGO-Ni	-34.09	3.00	30	6
Core-shell Ni@graphene	-31.42	4.25	30	7
NiO/CNTs composites	-25.40	2.00	20	8
MWCNTs/ferrite composites	-18.17	5.00	40	9
h-Ni(245)/GN nanocomposites	-17.80	5.00	60	10
$ZnFe_2O_4$@ZnO@rGO nanocomposites	-35.20	2.00	30	11
n-$FeNi_3$/GN nanocomposites	-29.00	5.00	60	12
Ti_3C_2Tx@RGO composite aerogel	-31.20	3.05	15	13
Fe_3O_4/RGO	-22.70	3.00	30	14
$Ni_{0.5}Co_{0.5}Fe_2O_4$/graphene	-30.92	4.00	50	15
$CoFe_2O_4$ rugbies/graphene composites	-39.00	2.00	60	16
C@$NiCo_2O_4$@Fe_3O_4	-43.00	3.40	60	17
RGO/ZnO hollow spheres	-45.05	2.20	50	18
N-SA/Ni-6%	-42.20	2.00	50	19
Ni-SA@NRGA	-49.46	2.00	25	This Work

References

[1] Yan J, Huang Y, Liu X D, Zhao X X, Li T H, Zhao Y and Liu P B 2021 *Polym. Rev.* **61** 646

[2] Zhang X, Xu J, Liu X Y, Zhang S, Yuan H R, Zhu C L, Zhang X T and Chen Y J 2019 *Carbon* **155** 233

[3] Wang K F, Chen Y J, Li H, Chen B B, Zeng K, Chen Y L, Chen H C, Liu Q L and Liu H Z 2019 *ACS Appl. Nano Mater.* **2** 8063

[4] Yan S J, Wang L N, Wang T H, Zhang L Q, Li Y F and Dai S L 2016 *Appl. Phys. A* **122** 235

[5] Huang Y W, Wang Y J, Wei S C, Liang Y, Huang W, Wang B and Xu B S 2019 *Int. J. Mod. Phys.* B **33** 1940055

[6] Li J, Bi S, Mei B, Shi F, Cheng W L, Su X J, Hou G L and Wang J J 2017 *J. Alloys Comp.* **717** 205

[7] Liu Y, Zhang X Y, Chen X, Wu Y X, Zhang C L, Wang J, Ji J Land Li K X 2021 *J. Mater. Chem. C* **9** 4910

[8] Wang J, Jia X L, Wang T H, Geng S, Zhou C, Yang F, Tian X J, Zhang L Q, Yang H T and Li Y F 2016 *J. Alloys Comp.* **689** 366

[9] Sun Z G, Qiao X J, Wan X, Ren Q G, Li W C, Zhang S Z and Guo X D 2016 *Appl. Phys. A* **122** 87

[10] Chen T T, Deng F, Zhu J, Chen C F, Sun G B, Ma S L and Yang X J 2012 *J. Mater. Chem.* **22** 15190

[11] Li F, Zhuang L, Zhan W W, Zhou M X, Sui G, Zhou A S, Bai G, Xiao W, Yang X P 2020 *Ceram. Int.* **46** 21744

[12] Ma T, Yuan M W, Islam S M, Li H F, Ma S L, Sun G B and Yang X J 2016 *J. Alloys Compd.* **678** 468

[13] Wang L B, Liu H, Lv X L, Cui G Z and Gu G X 202*0 J. Alloys Compd.* **828** 154251

[14] Wu J M, Ye Z M, Liu W X, Liu Z F and Chen J 2017 *Ceram. Int.* **43** 13146

[15] Yin P F, Deng Y, Zhang L M, Wu W J, Wang J, Feng X, Sun X Y, Li H Y and Tao Y 2018 *Ceram. Int.* **44** 20896

[16] Zhang S L, Jiao Q Z, Hua J, Li J J, Zhao Y, Li H S and Wu Q 2015 *J. Alloys Comp.* **630** 195

[17] Wei S A, Wang X X, Zhang B Q, Yu M X, Zheng Y W, Wang Y and Liu J Q 2017 *Chem. Eng. J.* **314** 477

[18] Han M K, Yin X W, Kong L, Li M, Duan W Y, Zhang L T and Cheng L F 2014 *J. Mater. Chem. A* **2** 16403

[19] Gao S S, An Q D, Xiao Z Y, Zhai S R and Yang D J 2018 *ACS Appl. Nano Mater.* **1** 5895